Multiple Mechanical Gradients are Responsible for the Strong Adhesion of Spider Attachment Hair

Silja Flenner, Clemens F. Schaber,* Igor Krasnov, Hergen Stieglitz, Martin Rosenthal, Manfred Burghammer, Stanislav N. Gorb, and Martin Müller*

Wandering spiders climb vertically and walk upside-down on rough and smooth surfaces using a nanostructured attachment system on their feet. The spiders are assumed to adhere by intermolecular van der Waals forces between the adhesive structures and the substrate. The adhesive elements are arranged highly ordered on the hierarchically structured attachment hair (setae). While walking, it has been suggested that the spiders apply a shear force on their legs to increase friction. However, the detailed mechanical behavior of the hair's structures during attachment and detachment remains unknown. Here, gradients of the mechanical properties of the attachment hair on different length scales that have evolved to support attachment, stabilize adhesion in contact, and withstand high stress at detachment, examined by in situ experiments, are shown. Shearing helps to self-align the adhesive elements with the substrate. The study is anticipated to contribute to the development of optimized artificial dry adhesives.

Animals such as spiders and geckos are able to attach to vertical surfaces and walk upside-down without the use of glue.[1–3] These dry attachment systems have evolved separately in different animal lineages to remarkably similar structures.[4] The spider attachment hair is part of the exoskeleton and consist of an amorphous protein matrix with embedded polymeric chitin molecules.[2,5,6] The attachment system of wandering

S. Flenner, H. Stieglitz, Prof. M. Müller
Helmholtz-Zentrum Geesthacht
Max-Planck-Str. 1, Geesthacht 21502, Germany
E-mail: martin.mueller@hzg.de
S. Flenner, Dr. I. Krasnov, H. Stieglitz, Prof. M. Müller
Institute of Experimental and Applied Physics
Kiel University
Kiel 24098, Germany
Dr. C. F. Schaber, Prof. S. N. Gorb
Functional Morphology and Biomechanics
Zoological Institute
Kiel University
Kiel 24098, Germany
E-mail: cschaber@zoologie.uni-kiel.de
Dr. M. Rosenthal, Dr. M. Burghammer
European Synchrotron Radiation Facility (ESRF)
71, avenue des Martyrs, CS 40220, Grenoble Cedex 9 38043, France

spiders is built up hierarchically. Their feet are covered with thousands of small attachment hair (setae), each covered by smaller hair (microtrichia) with widened platelet-like ends (spatulae) (Figure S1, Supporting Information). These spatula-shaped microtrichia are mainly present in the tip region on one side of the hair[7] and enable the spider to attach and detach in a fast and effortless way, which has been of particular interest in recent studies.[8,9]

When the spider puts its foot on the ground, a shear force pointing towards the spider's body is applied on the attachment setae. This is thought to bring the side with the ≈1 µm wide and 20 nm thin adhesive spatulae into contact with the surface.[2,10] The attractive force acting between the spatulae and a surface is assumed to be the short-range intermolecular van der Waals force.[3,11] It was proposed that—when lifting the foot—the spider pushes the leg away from the body so that the spatulae are peeled off the surface and the attachment hair detach.[8,10] However, the exact arrangement and alignment of the microtrichia and the spatulae during the attachment and the adhesive forces involved remained unknown.

In this study, we investigated the attachment process of single setae in situ with high spatial resolution and visualized the delicate cuticular structures and their changes at different stages and contact geometries. For this purpose, we used scanning nanobeam X-ray diffraction (XRD) and small-angle X-ray scattering (SAXS) to reveal changes also of the inner structure of fresh, chemically untreated attachment hair of the wandering spider *Cupiennius salei*. This species is a model organism for the mechanical properties of spider cuticle,[2,6,12] among other topics.[13] The scanning technique enables the evaluation of a diffractogram at each step regarding XRD/SAXS intensity and orientation, resulting in maps, where each pixel represents a single parameter calculated from the data. While the intensity data is directly correlated to the amount of (oriented) structures in the beampath, the orientation of the SAXS signal is perpendicular to the orientation of structures in the ≈100 nm range (e.g., nanofibrils, chitin-protein fibers).[2] Since the microtrichia are in the corresponding length scale, the SAXS signal is supposedly directly caused by these. Using this technique, there was no need for further preparation methods such as coating or slicing. For the measurement of the forces involved in the attachment process, the up to 1.5 mm long hair were glued onto the tip of a force sensing cantilever and
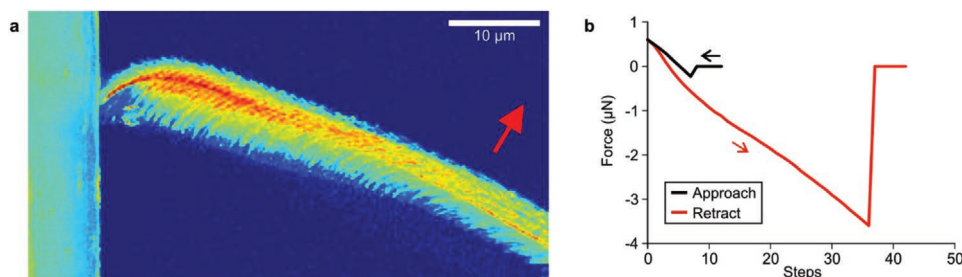
Figure 1. Attachment of a single hair. a) SAXS intensity map of an attachment hair (side view) adhering to a glass surface. The hair consists of a backbone with branching microtrichia supporting the spatula-shaped adhesive terminal structures, which are mainly present on the bottom of the hair. In the attachment process shown, only the tip of the hair contacts the surface. The arrow indicates the direction of pulling to obtain the retraction force curve in (b). b) Force measurement of an attachment and detachment cycle of the hair shown in (a). A small attractive force of −0.2 μN in the approach curve indicated the snap-in of the hair to the glass surface. Then the seta was slightly pushed onto the surface with a maximum force of +0.6 μN. The maximum adhesion force measured from the retraction curve before detachment was −3.6 μN.

attached and detached using a micromanipulator during the X-ray experiments.

The SAXS signals contain information about orientation and contrast of structures in the 100 nm range directly corresponding to the spatial scanning resolution. Here, the intensity map of the SAXS signals showed that the structure of a single spider attachment hair consists of a shaft (backbone) and the microtrichia (**Figure 1**a). The backbone of the hair bends at the tip. The density of the microtrichia gradually decreases from the tip towards the more basal parts of the hair. The angle of the microtrichia increases from more flat proximally to approximately perpendicular in the tip region. This arrangement can be interpreted as an adaptation for effective attachment of the adhesive structures on the tips of the microtrichia by their exposure for immediate contact with a surface during locomotion.

Without the need of strongly pushing them onto a surface, the hair easily stick well to surfaces with high attachment forces. In the example shown in Figure 1b, when the hair was close to the surface but not yet in contact, there was a small attractive snap-in force peak. Then, the hair was slightly pushed further against the glass surface. While detaching the hair by pulling in the opposite direction, the resulting force curve was not linear, likely because the hair was slightly bent (Movie S1, Supporting Information). The maximum adhesive force was 3.6 μN. This example may represent a nonideal attachment geometry as only the very tip of the hair adhered to the surface and the adhesive spatulae are mainly present on the bottom of the hair. However, when we assume a total number of 18 800 setae per spider (2350 setae per leg),[14] the adhesion force of 3.6 μN per seta would be enough to hold an adult female spider with a typical weight of 3.5 g on the ceiling with half of its attachment hair in contact.

Attaching the hair to a surface in top view showed that the overall shape and the orientation of the microtrichia and spatulae, calculated from the SAXS signals, changed from the freestanding to the attached state. As also seen in the XRD signal map, the hair was clearly narrower in the attached state (**Figure 2**a,b). The microtrichia that were visibly branching off the backbone in the freestanding hair (Figure 2a) were no longer visible in their full dimension in the attached hair (Figure 2b), which indicates that they were attracted towards the surface. In single data points on both sides of the hair, the angular orientation of the structures changed by up to

90°, which points to the alignment of single contact elements with the surface (Figure 2c,d). The mean orientation of all the structures did not change (from 103° to 104° only) significantly from the freestanding to the attached hair. However, the observed decrease in the standard deviation of the orientation from 43° to 39° may point to a higher degree of structural alignment. A further indication for this increased alignment was the decrease of the two peaks at 51° (± 3°) and 171° (± 3°) in the angular orientation frequency distribution of the structures of the freestanding hair when it was attached (Insets Figure 2c,d).

In side view, the structural features of the attachment hair could be differentiated more clearly. A further single hair was attached with apparently all the adhesive spatulae on its tip in contact. **Figure 3**a–e shows the mapped SAXS intensity at different stages of attachment and detachment. The corresponding force curve is depicted in Figure 3f. First, the hair was pushed against the glass surface (Figure 3a). Before contact, the microtrichia were oriented towards the surface so that the adhesive spatulae on their tips could then efficiently adhere at first contact. In the second step, pulling the hair vertically led to the flattening of the hair tip region and proper surface contact of all the spatulae (Figure 3b). Directly at the interface between the hair and the surface, at the end of the microtrichia, the intensity of the SAXS signal increased strongly. This result points to surface contact of the spatulae and their alignment perpendicular to the X-ray beam, leading to increased scattering. Trying to detach the hair made the microtrichia tilt in contact and the backbone came closer to the surface (Figure 3c,d). Finally, most of the microtrichia detached at a force of 25 μN and the hair slipped on the surface with the adhesive elements of the tip still in contact (Figure 3e). Completely pulling off the seta from the surface still resulted in an adhesive force of 1.6 μN before detachment. Interestingly, the microtrichia remained tilted, maybe caused by viscous deformation during the 18 h long X-ray experiment. The nonlinearity of the force curve at pulling-off (Figure 3f) again indicated the bending of the hair as marked in Figure 3c,d. This bending ensures that the adhesive spatulae stay in contact with the surface at increasing pulling forces and is likely caused by the structural gradient in the hair backbone.[3] The maximum adhesion force of 25 μN results in a safety factor of ≈13 for an adult female spider, if all attachment hair were in contact with a surface.

**ADVANCED
SCIENCE NEWS**

www.advancedsciencenews.com
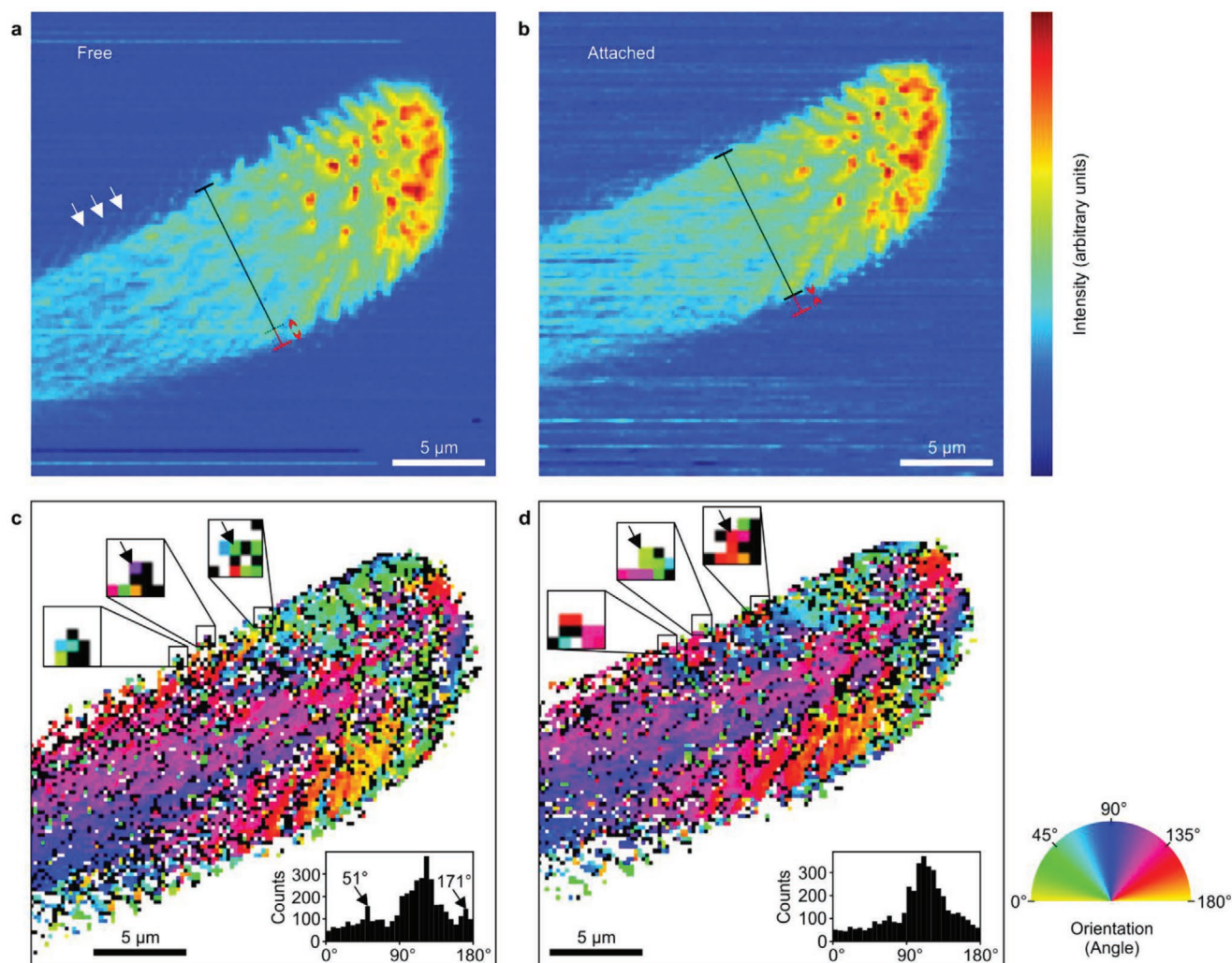
**ADVANCED
MATERIALS**

www.advmat.de

Figure 2. a,b) Top view of an attachment hair freestanding and attached. Intensity of the wide-angle XRD signal of the freestanding (a) and the same hair attached to an X-ray translucent Si_3N_4 surface (b). The lines indicate the difference of width of the hair backbone. Single microtrichia branching from the backbone are clearly visible in (a) (arrows) and hardly visible in (b), which points to their reorientation and adhesion to the surface. c,d) Angular orientation of the structures calculated from the SAXS signal of the freestanding (c) and the attached hair (d). The color half-circle on the right indicates the orientation of the structures. The insets exemplarily show magnified $1 \times 1\,\mu m^2$ large areas and identified pixels (arrows) with a large angular change upon attachment, likely indicating the alignment of single spatulae or microtrichia. In black pixels, no predominant orientation could be measured. Note that each single pixel represents the data from all the structures exposed to the X-ray beam in each single step of scanning the sample.

Different regions of the adhesive tip showed different deformation behavior under the tensile stress during pulling as shown by the mapped orientation of the structures calculated from the SAXS signals (Figure 3g–k). The mean orientation was calculated for five different regions of the microtrichia at three different steps of detachment (Figure 3h–j,l). At 0.4 μN tensile force, the angle of the microtrichia was 47° next to the backbone in region 3 (Figure 3h), 59° in region 2, and 62° next to the surface in region 1. Up to the force of 11.6 μN, the angles in these three regions changed linearly with gradually different slopes (Figure 3l), which indicates bending of the microtrichia relative to the backbone. The maximum slope pointing to the most structural flexibility was found in the region next to the surface. This facilitates the alignment of the contact elements with the surface. In region 4 the total angular change was

similar to region 1 and larger than in the neighboring region 5 that was similar to region 2. The nonlinearity of the deformation in regions 4 and 5 could be caused by a kind of unfolding of the microtrichia of the very tip region during the force step between 0.4 and 2.0 μN.

The flexibility of the microtrichia in contact is caused by their specific structural gradient and bending stiffness from plate-like and membranous in the spatula to rod-like in the stalk supporting it. When attached, the spatulae firmly stick to the place in contact whereas the approximately 5 μm long stalk can bend under load. Similar mechanical effective gradients have been found in several animal attachment systems and are essential for their function.[15] In the hairy attachment systems, a stiff base of the setae prevents the adhesive structures to stick to each other. Easily deformable structures on the tips allow for
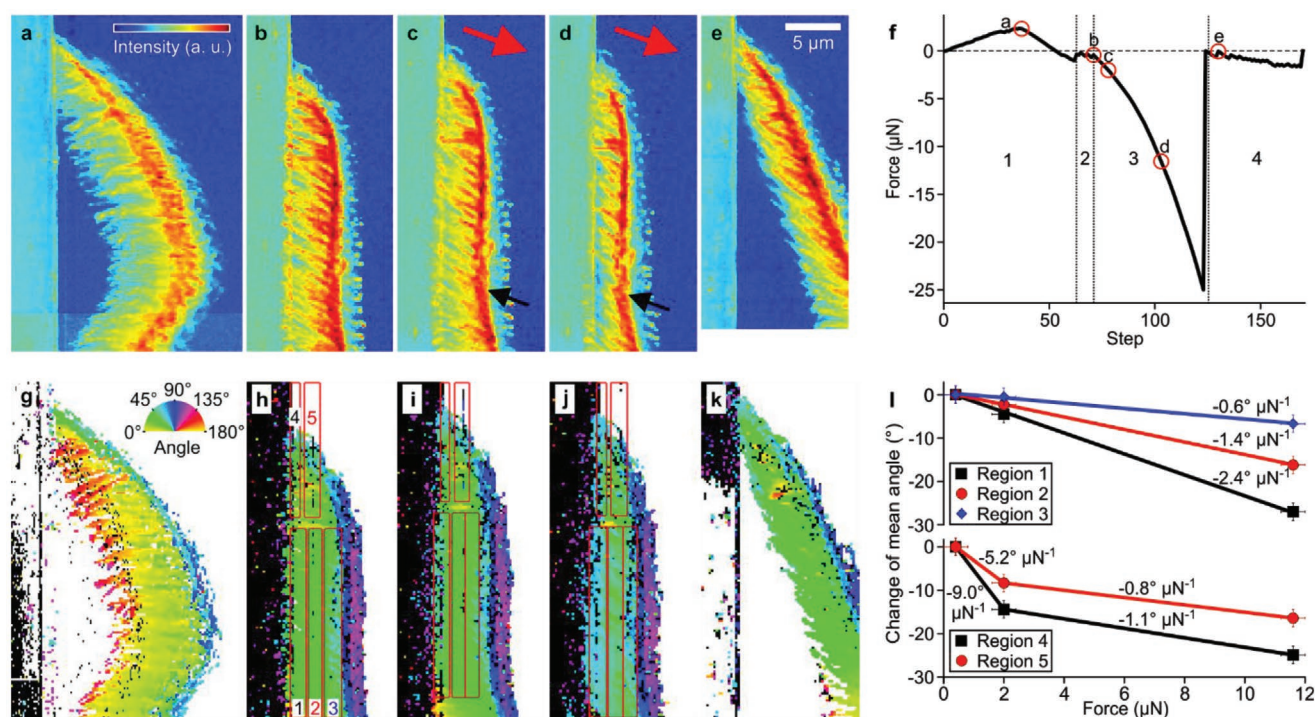
**ADVANCED
SCIENCE NEWS**

www.advancedsciencenews.com

**ADVANCED
MATERIALS**

www.advmat.de

Figure 3. Side view of an attachment hair during force-controlled attachment and detachment experiments. a–e) SAXS intensity maps in different states of contact corresponding to the points marked (a)–(e) in the force curve in (f). a) Hair tip in contact with the surface after loading, b) adhesive microtrichia aligned with the surface after shearing the hair vertically downwards, c) pulling on the seta by 2.0 µN (force direction as indicated by the large arrow), d) further pulling on the seta that resisted with an adhesive force of 11.6 µN, e) tip adhering after detachment of the majority of the microtrichia and slight slipping. Note the bending of the backbone marked by the black arrows in (c) and (d). f) Force measured during the attachment/detachment experiments. The red circles correspond to the images shown in (a)–(e) and (g)–(k). The numbers mark the different experimental regimes separated by the vertical dotted lines as follows. (1) Approaching the surface and retracting, followed by a small detachment event; (2) moving the hair in contact vertically downward, resulting in alignment of the adhesive spatulae of the microtrichia with the surface; (3) pulling on the strongly adhering seta, until a large drop of adhesive forces indicated detachment; (4) retracting the hair still in contact with its tip followed by the loss of contact. g–k) Structure orientation maps corresponding to (a)–(f). h–j) The red boxes indicate the five regions for which the mean of angular orientation was calculated. l) Mean angular orientation change (± uncertainty) of the structures in the five different regions marked in (h)–(j). The horizontal error bars indicate the uncertainty of the force values. In the upper part of the figure that shows the linear orientation changes in regions (1)–(3), the slopes of the linear regression lines are indicated. In the lower part of the figure, the slopes for the angular changes of regions (4) and (5) are given separately for the single force steps

their alignment with a surface and thereby increase the contact area and adhesive force. In insects, such as, e.g., the ladybird beetle, it was shown that in the setae of the attachment system the structural gradient from round to flat goes along with a gradient in the material properties (Young's modulus) of the cuticle from stiff (6.8 GPa) at the base to very soft (1.2 MPa) at the tip.[16] In the spider adhesive hair, an additional structural gradient from hollow tube-shaped to flat has been found along the axial direction of the hair.[2] Up to now, in the dry attachment systems of the spiders and the geckos no gradient in the material composition has been found. Here, the gradients in the mechanical properties are thought to be purely caused by gradients induced by the size variation of the structures, and consequently different bending stiffness, although an additional tuning of the adhesive function by the arrangement of charged proteins in the setae of the gecko has been discussed.[17]

Using scanning nanobeam XRD/SAXS and sub-micro-newton force-resolved manipulation allowed for the simultaneous characterization of changes of the structures of the attachment hair and the mechanical properties. Our results

show that the adhesive forces of an attachment hair strongly depend on the contact geometry with the surface. The geometry with only the tip adhesive elements in contact yielded a safety factor of 2, hardly enough for the spider to walk upside-down. In the geometry with all the adhesive elements of a hair in contact, the safety factor was 13. Such a geometry is established when increased shear forces promote the alignment of more adhesive contact elements with the surface, and therefore increased contact area and adhesion force. The arrangement of the adhesive spatulae can be thought of a structure, which ensures adhesion under critical scenarios such as slipping. The deformation patterns of the hair and the contact elements allow for proper adhesion at high tensile stress. The structural arrangement and the resulting gradient of the mechanical properties—both hierarchical on several length scales—make the attachment hair stable and durable for attachment and detachment at every step of the walking spider. They could be an excellent model for the development of new high-performance residue-free artificial adhesive materials, e.g., based on carbon nanotubes[18] or other natural nanofibers.[19]

2002758 (4 of 6)

**ADVANCED
SCIENCE NEWS**

www.advancedsciencenews.com

**ADVANCED
MATERIALS**

www.advmat.de

Experimental Section

Sample Preparation: Single attachment hair (setae) were picked from second and third walking legs of specimens of the large Central American hunting spider *C. salei* in the middle of the pretarsal claw tuft. The animals were obtained from the breeding stock of the Department of Neurobiology of the University of Vienna (Austria). The results were gained from hair of legs separated from the spider not longer than five days and kept in a fridge whenever possible. To prevent drying out, the legs were sealed at their autotomy site on the trochanter using a mixture of slightly heated beeswax and colophony. For the top view arrangement, single hair was mounted freestanding onto the tip of a sharpened glass capillary using two-component polysiloxane (Coltene light body, Coltène/Whaledent AG, Altstätten, Switzerland). For the side view arrangement, the hair was mounted on the tip of a force-sensing cantilever (FMT-400, Kleindiek Nanotechnik GmbH, Reutlingen, Germany).

Sample Manipulation: For the experiments, the samples were attached to a three-axis micromanipulator (MM3A, Kleindiek Nanotechnik GmbH, Reutlingen, Germany) that had a resolution in the low nanometer-range. For top view in situ attachment, the tip of the attachment hair was slightly pushed onto a 200 nm thick silicon nitride membrane window (Silson Ltd., Southam, United Kingdom) oriented perpendicular to the X-ray beam. In side view, the samples were attached and detached to a vertically mounted borosilicate glass capillary with a diameter of 1 mm. The analogue signal of the force sensor was converted and continuously recorded to a computer hard disk.

Nanobeam X-Ray Diffraction and Scattering: The experiments were performed at the nanofocus extension EH III of the beamline ID13 at the European Synchrotron Radiation Facility ESRF. The beam was generated by an undulator, monochromized by a Si-111 double monochromator and focused using refractive lenses. The diffractograms were recorded in a combined wide-angle XRD and SAXS setup. Scanning was achieved by moving the sample two-dimensionally in a grid-shaped pattern. For the top view measurements, a FReLoN detector camera (ESRF, Grenoble, France) was used at a distance of 94.1 mm from the sample. The wavelength was 0.8349 Å. The X-ray beam was focused to a size of ≈250 × 250 nm^2. An area of 30 × 30 μm^2 was scanned in a grid with a step size of 250 nm with an exposure time of 1 s per step. The resulting maps consisted of 14 641 single diffractograms each. For the side view measurements, the diffractograms were recorded using an Eiger X 4M detector (Dectris Ltd., Baden-Daetwill, Switzerland) at a distance of 203.5 mm to the sample. To minimize scattering by air molecules, the distance between the sample and the detector was bridged by a helium-filled flight-tube. The wavelength of the X-ray beam was 0.847 Å. The beam was focused to a size of ≈150 × 150 μm^2. The scanning grid step size was set to 200 nm and X-ray exposure time per step was 0.5 s. Images were taken at significant steps of attachment and detachment of the seta.

Data Analysis: The data analysis and calibration were performed using the Python software library pyFAI for fast azimuthal integration. After background subtraction, each diffractogram from the 2D scans was evaluated regarding wide-angle XRD, SAXS intensity, or SAXS intensity and orientation. To obtain the intensity, the signals were integrated in azimuthal direction. To obtain the orientation of the fibrous structures, which is perpendicular to the orientation of the SAXS signal, the SAXS signal was integrated in radial direction. The data of the integration were fitted, and the peaks of this fit indicated the orientation of the signal (Figure S2, Supporting Information). Finally, the data were plotted in a grid representing the physical dimensions of the scanned area to obtain the intensity and orientation maps. If no predominant orientation of the SAXS signal could be found, this is represented as black pixels in the maps.

Supporting Information

Supporting Information is available from the Wiley Online Library or from the author.

Conflict of interest

The authors declare no conflict of interest.

[1] a) E. Arzt, S. Gorb, R. Spolenak, *Proc. Natl. Acad. Sci. USA* **2003**, *100*, 10603; b) A. B. Kesel, A. Martin, T. Seidl, *J. Exp. Biol.* **2003**, *206*, 2733.

[2] C. F. Schaber, S. Flenner, A. Glisovic, I. Krasnov, M. Rosenthal, H. Stieglitz, C. Krywka, M. Burghammer, M. Müller, S. N. Gorb, *J. R. Soc., Interface* **2019**, *16*, 20180692.

[3] K. Autumn, Y. A. Liang, S. T. Hsieh, W. Zesch, W. P. Chan, T. W. Kenny, R. Fearing, R. J. Full, *Nature* **2000**, *405*, 681.

[4] A. Filippov, V. L. Popov, S. N. Gorb, *J. Theor. Biol.* **2011**, *276*, 126.

[5] F. G. Barth, *Cell Tissue Res.* **1973**, *144*, 409.

[6] a) Y. Politi, M. Priewasser, E. Pippel, P. Zaslansky, J. Hartmann, S. Siegel, C. Li, F. G. Barth, P. Fratzl, *Adv. Funct. Mater.* **2012**, *22*, 2519; b) C. Valverde Serrano, H. Leemreize, B. Bar-On, F. G. Barth, P. Fratzl, E. Zolotoyabko, Y. Politi, *J. Struct. Biol.* **2016**, *193*, 124.

[7] a) S. Niederegger, S. N. Gorb, *J. Comp. Physiol., A* **2006**, *192*, 1223; b) J. O. Wolff, S. N. Gorb, *J. Exp. Biol.* **2012**, *215*, 179; c) S. Niederegger, in *Spider Ecophysiology*, (Ed.: W. Nentwig), Springer, Berlin, Germany **2013**, p.57.

[8] J. O. Wolff, S. N. Gorb, *Sci. Rep.* **2013**, *3*, 1101.

[9] a) E. Wohlfart, J. O. Wolff, E. Arzt, S. N. Gorb, *J. Exp. Biol.* **2014**, *217*, 222; b) J. O. Wolff, W. Nentwig, S. N. Gorb, *PLoS One* **2013**, *8*, e62682; c) K. F. Frost, S. N. Gorb, J. O. Wolff, *Zool. Anz.* **2018**, *273*, 231.

[10] S. N. Gorb, *Attachment Devices of Insect Cuticle*, Kluwer Academic Press, Dordrecht, The Netherlands **2001**.

[11] a) K. Autumn, A. M. Peattie, *Integr. Comp. Biol.* **2002**, *42*, 1081; b) K. Autumn, M. Sitti, Y. A. Liang, A. M. Peattie, W. R. Hansen, S. Sponberg, T. W. Kenny, R. Fearing, J. N. Israelachvili, R. J. Full, *Proc. Natl. Acad. Sci. USA* **2002**, *99*, 12252.

[12] a) M. E. McConney, C. F. Schaber, M. D. Julian, F. G. Barth, V. V. Tsukruk, *J. R. Soc., Interface* **2007**, *4*, 1135; b) M. E. McConney, C. F. Schaber, M. D. Julian, W. C. Eberhardt, J. A. C. Humphrey, F. G. Barth, V. V. Tsukruk, *J. R. Soc., Interface* **2009**, *6*, 681; c) M. Erko, M. A. Hartmann, I. Zlotnikov, C. Valverde Serrano, P. Fratzl, Y. Politi, *J. Struct. Biol.* **2013**, *183*, 172; d) S. L. Young, M. Chyasnavichyus, M. Erko, F. G. Barth, P. Fratzl, I. Zlotnikov, Y. Politi, V. V. Tsukruk, *Acta Biomater.* **2014**, *10*, 4832; e) M. Erko, O. Younes-Metzler,

**ADVANCED
SCIENCE NEWS**

www.advancedsciencenews.com

**ADVANCED
MATERIALS**

www.advmat.de

A. Rack, P. Zaslansky, S. L. Young, G. Milliron, M. Chyasnavichyus, F. G. Barth, P. Fratzl, V. Tsukruk, I. Zlotnikov, Y. Politi, *J. R. Soc., Interface* **2015**, *12*, 20141111; f) S. L. Young, M. Chyasnavichyus, F. G. Barth, I. Zlotnikov, Y. Politi, V. V. Tsukruk, *Acta Biomater.* **2016**, *41*, 40; g) M. Tadayon, O. Younes-Metzler, Y. Shelef, P. Zaslansky, A. Rechels, A. Berner, E. Zolotoyabko, F. G. Barth, P. Fratzl, B. Bar-On, Y. Politi, *Adv. Funct. Mater.* **2020**, *30*, 2000400.

[13] a) F. G. Barth, *A Spider´s World: Senses and Behavior*, Springer, Berlin, Germany **2002**; b) P. Fratzl, F. G. Barth, *Nature* **2009**, *462*, 442; c) C. F. Schaber, F. G. Barth, *J. Comp. Physiol. A* **2015**, *201*, 235.

[14] J. O. Wolff, S. N. Gorb, *Arthropod Struct. Dev.* **2012**, *41*, 419.

[15] a) S. N. Gorb, A. E. Filippov, *Beilstein. J. Nanotechnol.* **2014**, *5*, 837; b) L. Heepe, S. Höft, J. Michels, S. N. Gorb, *Soft Matter* **2018**, *14*, 7026; c) P. Perez Goodwyn, A. Peressadko, H. Schwarz, V. Kastner, S. N. Gorb, *J. Comp. Physiol. A* **2006**, *192*, 1233.

[16] H. Peisker, J. Michels, S. N. Gorb, *Nat. Commun.* **2013**, *4*, 1661.

[17] L. Alibardi, *Protoplasma* **2018**, *255*, 1785.

[18] C. F. Schaber, T. Heinlein, G. Keeley, J. J. Schneider, S. N. Gorb, *Carbon* **2015**, *94*, 396.

[19] C. F. Schaber, A. Kreitschitz, S. N. Gorb, *ACS Appl. Mater. Interfaces* **2018**, *10*, 37566.